Photometry with the Tractor

Jesse Jedrusiak

Contents

1 Introduction **2**

2 the Tractor **2**

3 Methods **2**
3.1 Priors . . . 2
3.1.1 Source Priors . . . 2
3.1.2 Images Priors . . . 4
3.1.3 PSF/PRF Priors . . . 4
3.2 Source Extraction . . . 5
3.3 Error Estimation . . . 6

4 Results and Discussion **6**
4.1 Comparison with Existing Catalogs . . . 6
4.1.1 Photometry . . . 6
4.1.2 Flux Error . . . 11
4.2 Failure Indications . . . 11
4.3 Failed Methods . . . 17

5 Summary **17**

6 Examples **17**

1 Introduction

In this short article, I will introduce THE TRACTOR code and the latest method in which I used THE TRACTOR to extract IRAC channel 1, 2, 3, 4, and MIPS 24 μm fluxes. I'll discuss how my estimated fluxes compare to the catalog values, speculate reasons for the discrepancies, examine how one might determine where the method fails, and briefly discuss previously attempted techniques. All magnitudes are given as AB magnitudes.

2 THE TRACTOR

Fluxes were extracted using THE TRACTOR code (D. Lang et al. 2016, in preparation). In general, THE TRACTOR uses prior knowledge about the images and sources to optimize the likelihood for catalog properties. Input image parameters include a noise model, a PSF model, image WCS, photometric calibrations, and sky level. The input source parameters include the source positions, brightnesses, surface brightness profiles, and projected elliptical shapes. THE TRACTOR proceeds by rendering the source model convolved with the image PSF model and performs a least squares fit to the image data.

THE TRACTOR is merely a *Python* library and so does not have a front end user interface. Rather, the user must write their own driver script to implement the objects in the library. This allows the user to write their own customized photometry code using the powerful probabilistic fitting features that THE TRACTOR has to offer. In practice, the user's driver script inputs all prior image information into the " Tractor Image" class, and all prior source information into the "Tractor Source" class. These two objects are inherited by the final "Tractor" object/class which is then optimized.

3 Methods

3.1 Priors

My implementation of THE TRACTOR requires prior knowledge of each source's position, the per-pixel noise and background of the science image, and the PSF/PRF of each bandpass. The specific method assumes the sources are unresolved, which is valid for the high-z sample used in this analysis. The code also requires that the user provide a prior flux, however this flux can be initialized to unity with no effect on the resulting photometry. I chose to use the catalog fluxes of the sources in each bandpass as the prior fluxes for the purpose of comparing THE TRACTOR fluxes to the catalog values. Below I describe how each of these priors were obtained for my sample.

3.1.1 Source Priors

I began with 1721 IRAC sources from the Spitzer Extragalactic Representative Volume Survey (SERVS) in the XMM-LSS field. The sources were selected to have H - $m_{3.6} > 1.6$ (HIEROs) and/or K_S - $m_{4.5} > 1.6$ (KIEROs) (Sajina et al., in preparation). A catalog containing the positions and redshifts of the H/KIEROs was provided to me by Professor Anna Sajina.

I obtained more accurate K_S position priors by source matching the H/KIERO catalog to the VISTA Deep Extragalactic Observations (VIDEO) Survey DR2 K_S-selected catalog using a matching radius of 1.5" ($\sim>$ FWHM$_{\rm IRAC}$/2). The offsets between the H/KIERO position and the VIDEO K_S position are given in Figure 1. The median offset is ~ 0.045". I adopted the K_S counterpart position as the position prior for the >99 % of H/KIEROs with K_S catalog counterparts. I adopted the H/KIERO positions as the position priors for the remaining 9 sources without K_S catalog counterparts. I inspected the K_S image at the positions of sources without catalog counterparts and found there were clearly sources at these positions, but they are

fainter than the $K_S < 24.5$ magnitude limit of the catalog.

I obtain flux priors for IRAC channels 1 and 2 by source matching the K_S positions of the H/KIEROs to the SERVS DR2 IRAC channels 1 and 2 catalogs using a matching radius of 1.5" ($\sim>$ FWHM$_{\rm IRAC}$/2). I find for both IRAC channels 1 and 2 that $\sim$ 82 % of my H/KIEROs have catalog counterparts from which I can obtain a flux prior. The $\sim$ 18 % of H/KIEROs without SERVS counterparts lie outside of the publically released area and so do not appear in the SERVS DR2 catalogs. The flux priors for sources without catalog counterparts are initialized to unity.

The flux priors for IRAC channels 3 and 4 were obtained by source matching the K_S positions of the H/KIEROs to the SWIRE DR2 band-merged catalog using the same matching radius as that used for IRAC channels 1 and 2 i.e. 1.5" ($\sim>$ FWHM$_{\rm IRAC}$/2). The SWIRE coverage area for IRAC channels 3 and 4 was divided into 16 tiles, 5 of which contained H/KIEROs. For the purposes of testing, I consider only those sources that lie in tile 1_2. While 1014 of the 1721 H/KIEROs lie in this tile, only 53 ($\sim$ 5 %) and 19 ($\sim$ 2 %) of the sources in this tile have channel 3 and 4 catalog counterparts, respectively. The flux priors for sources without catalog counterparts are initialized to unity.

MIPS 24μm flux priors were obtained by source matching the K_S positions of the H/KIEROs to the Vaccari et al. MIPS 24 μm catalog using a search radius of 3" ($\sim$ FWHM$_{\rm MIPS1}$/2). This catalog is deeper than the SWIRE catalogs and so provides more matches from which I can obtain flux priors. Of my 1721 H/KIEROs, 1568 of them lie within the SWIRE MIPS 24 μm coverage area. I found that $\sim$ 63 % of the H/KIEROs within this coverage area have a MIPS 24μm catalog counterparts. The flux priors for sources without catalog counterparts are initialized to unity.

For each bandpass, I created a priors catalog containing the prior positions and fluxes of the H/KIEROs. I appended to these catalogs all other K_S sources from the VIDEO K_S catalog that are within 6 $\times$ FWHM of each H/KIERO while being careful not to duplicate sources. This ensures that sources are fit at all K_S positions that lie within each subimage during the fitting procedure (Section 3.2). Flux priors for the appended sources are obtained using the same method described above for the H/KIEROs. The priors catalog for each bandpass is input into the fitting code.

The benefit of using THE TRACTOR is its ability to deblend sources. Here I define a source as being blended if there is more than one K_S catalog counterpart within the search radius defined above for each bandpass. I found that in each of the four IRAC channels $\sim$ 2 % of the H/KIEROs that lie within each channel's coverage area are expected to be blended. Of the H/KIEROs that lie within the MIPS channel 1 coverage area, $\sim$ 22 % are expected to be blended.

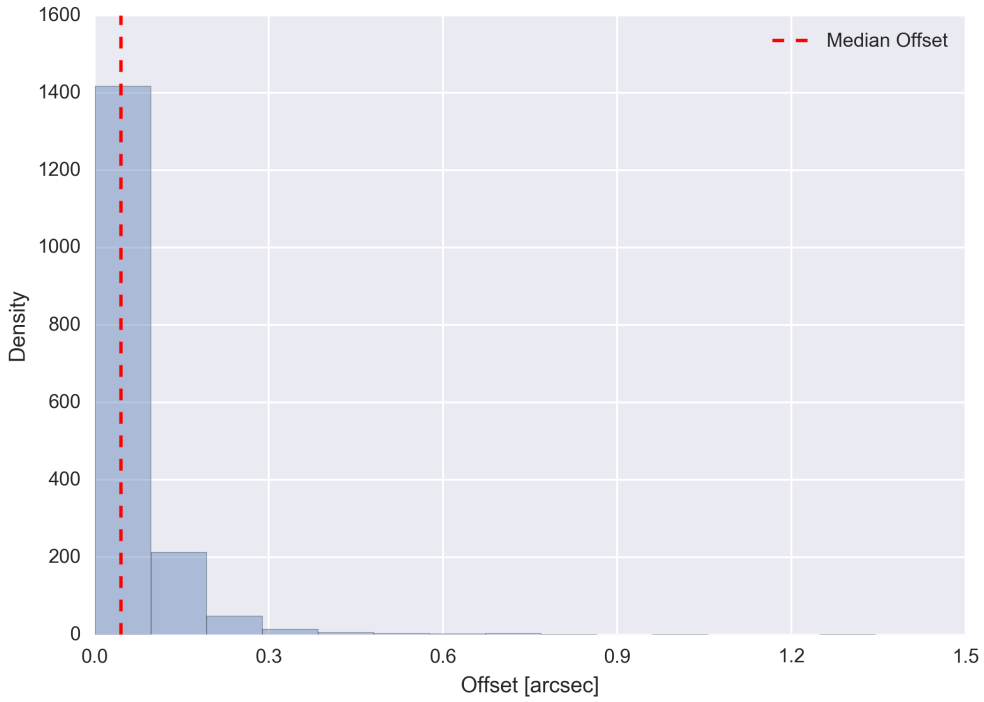

Figure 1: Offset between the H/KIERO position and the K_S catalog counterpart position. Note: the nine H/KIEROs without K_S catalog counterparts lie outside the bounds of this plot.

3.1.2 Images Priors

For IRAC channels 1 and 2 photometry, I made use of the SERVS DR2 IRAC channel 1 and 2 mosaics (Mauduit et al. 2012). For IRAC channel 3, channel 4, and MIPS 24μm photometry, I made use of the SWIRE DR4 mosaics (Surace et al. 2005). I obtained the per-pixel noise and sky background in these images by sampling the standard deviation and mean within empty apertures in several locations on the map. The properties of these maps are given in Table 1.

Bandpass	Mean [μJy/pix]	Median [μJy/pix]	Standard Deviation [μJy/pix]
IRAC 1	0.8327	0.8351	0.02106
IRAC 2	2.525	2.525	0.02567
IRAC 3	12.75	12.77	0.5216
IRAC 4	64.39	64.41	0.5650
MIPS 1	-0.3602	-0.3308	1.570

Table 1: The mean, median, and standard deviation of pixel values within several empty apertures for each bandpass. Note: The medians were not sampled at the same locations as the mean and standard deviation.

3.1.3 PSF/PRF Priors

PRFs for IRAC channels 1, 2, 3, and 4 were obtained from http://irsa.ipac.caltech.edu/. For channels 1 and 2, I use the "Warm" PRFs (Hora et al. 2012), while for channels 3 and 4, I use the "Core" PRFs (Hoffman et al. 2005). The MIPS 24 μm PRF used is from Gordon et al. (2008).

The channel 1 and 2 PRFs were rotated and interpolated to the header specifications of the SERVS images using Adam Ginsberg's *Python* implementation of `hcongrid`. An additional rotation of 180 degrees was needed for the PRF to match the appearance of stars selected from the SERVS catalogs. This is possibly due to the XMM field being in the southern hemisphere, but this is only speculation. Because of the format of the headers of the IRAC channel 3, 4 and MIPS 24 μm PRFs, it was more convenient to do the interpolation and centering using `change_image_scale.pro` and `ensure_psf_centered.pro` by Karl Gordon and J.D. Smith. The latter codes do not include the ability to handle the rotation of the PRFs so the PRFs for the longer wavelength channels examined here are not rotated to the same orientation as the science images. From my results, it appears this does not have a large effect as the PRFs at longer wavelengths are nearly rotationally symmetric. After all PRFs were interpolated to accommodate the specifications of the science images, they were normalized such that their flux was unity. The PSF/PRFs used in my fitting procedure are shown in Figure 2 .

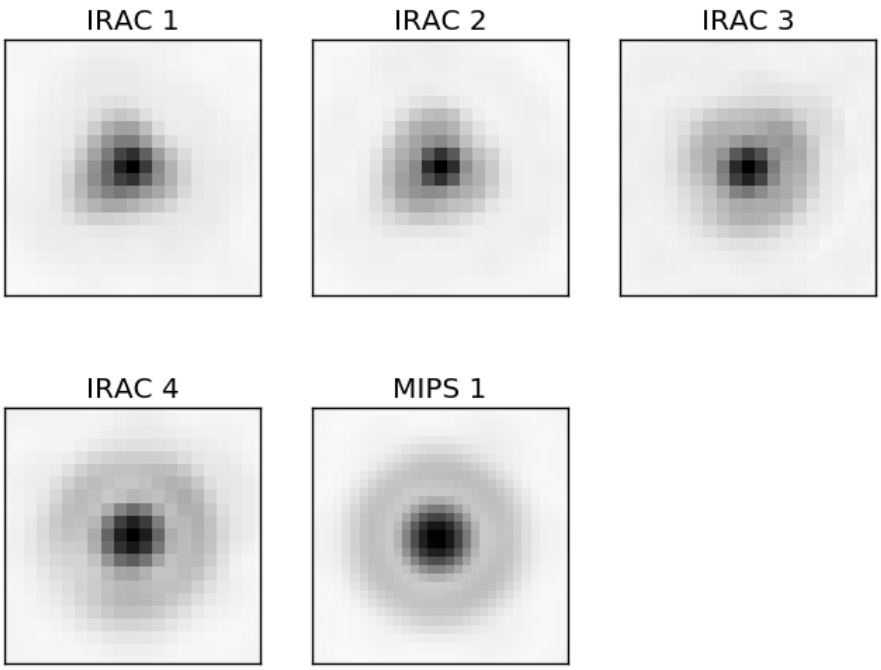

Figure 2: PRFs at the pixel scales of the science images. The images are square-root-scaled to enhance the visibility of the shape.

3.2 Source Extraction

My fitting code assumes all sources are unresolved, which for the H/KIEROs ($< z >\sim 2$) is true for all of the wavelengths considered here. This allows me to bypass the task of modeling the projected shapes and surface brightness profiles of the galaxies, and instead just assume them to be point sources. Point sources are fit at the positions of all K_S sources within and just outside a square subimage with side length $\sim 3 \times$ FWHM. All image and source parameters except for flux are held fixed during the fitting procedure.

The flux is returned in the units of the map $\times$ pixels. Values from the output catalogs, therefore, must be converted to standard units (e.g. μJy) for interpretation. For the *Spitzer* images, the map units are

[MJy/sr]; therefore, the flux is returned in units of [MJy/sr] × pixels. To obtain the flux in μJy I convert the map units of [MJy/sr] to [μJy/pixel]. This conversion factor is dependent on the image pixel scale and can be easily found to be:

$$1[MJy/sr] \approx 23.5044[\frac{\mu Jy}{arsec^2}] \times (\text{pixelscale}[arcsec/pixelside])^2 \quad (1)$$

For example, the IRAC channels 1 and 2 images have a pixel scale of 0.6 arcsec / pixel, yielding a multiplicative conversion factor with magnitude of 8.46. Fluxes are converted to AB magnitudes for comparison with the catalog values using the standard conversion below.

$$m_{AB} = -2.5\, log_{10}\left(\frac{flux\,[\mu\text{Jy}]}{3631 \times 10^6\,\mu\text{Jy}}\right) \quad (2)$$

3.3 Error Estimation

There are two components that constitute my estimation of the error: the contribution from noise to the extracted flux and the quality of the fit. For the first component, I used the obtained PSFs (Section 3.1.3) to derive the noise pixels associated with them so that I could estimate the error in the extracted fluxes associated with the noise contribution to the flux.

$$\sigma_F = \sigma_{PP} \times \sqrt{N} \quad (3)$$

Here σ_{PP} is the per-pixel noise sampled from the map, and N is the noise pixels defined as,

$$N = \frac{1}{\Sigma Pi^2} \quad (4)$$

where P_i is the value of the PSF in pixel i.

For the second component, I use the standard deviation of the fit (i.e. σ(image -model)) of the central source output by THE TRACTOR. I then add these two components in quadrature to estimate the total error in the extracted fluxes.

$$\sigma_{F,tot} = \sqrt{{\sigma_{F,noise}}^2 + {\sigma_{F,fit}}^2} \quad (5)$$

A comparison of my error estimates with those from the associated catalogs are presented in Table 4.

4 Results and Discussion

4.1 Comparison with Existing Catalogs

4.1.1 Photometry

Here I compare the THE TRACTOR fluxes in each bandpass to the catalog values. I'll also show that most of the disagreements in flux comparisons where the catalog flux is significantly greater than THE TRACTOR flux (Δm > σ) occur when the source is crowded. The results are summarized in Table 2, and plotted in Figures 3 through 7.

Bandpass	$\langle \Delta m \rangle$	$\widetilde{\Delta m}$	σ	$\langle \Delta m_{iso} \rangle$	$\widetilde{\Delta m_{iso}}$	σ_{iso}
IRAC 1	0.0507	0.0207	0.1333	0.0131	0.009	0.0626
IRAC 2	0.0307	0.0073	0.1164	-0.0012	-0.0034	0.0585
IRAC 3	0.2025	0.1734	0.1897	0.1747	0.1373	0.1898
IRAC 4	0.1861	0.1803	0.2036	0.1316	0.0252	0.2590
MIPS 1	0.1442	0.0986	0.6504	0.0394	0.0295	0.3736

Table 2: The mean, median, and standard deviation of the offsets between THE TRACTOR magnitudes and the catalog values. Values are given for the whole comparison sample as well as just for sources that are not blended/crowded (isolated).

My results are broadly consistent with the catalogs. I speculate that a fraction of the variance in Δm can be explained by my assumption of a constant sky background. This could also possibly explain the slight negative correlation between Δm and decreasing flux seen in all bandpasses.

A fraction of the SERVS data was taken prior to the final temperature stabilization of IRAC (Mauduit et. al 2012). The resulting calibration errors in the map were corrected at the catalog level by comparing the SERVS SEXTRACTOR fluxes to those of SWIRE (SERVS DR2 documentation). The affect was negligible for IRAC channel 2, but channel 1 SEXTRACTOR fluxes required a multiplicative correction factor of 1.02. It follows that if THE TRACTOR fluxes have been affected in a similar way (i.e. marginally reduced due to the map errors), then I expect some of the offset seen in the comparison of IRAC channel 1 fluxes to be a result of this. For example, if I were to assume the same multiplicative calibration factor (i.e. 1.02) for the channel 1 TRACTOR fluxes, the offsets would be reduced to $\langle \Delta m \rangle$ = 0.0292, and $\langle \Delta m_{iso} \rangle$ = -0.0084.

Channels 3 and 4 have the most significant disagreement. I believe this is likely due to the small number of sources that had catalog counterparts to compare to. I can only speculate until I can run the code across all of the channel 3 and 4 tiles and perform a more thorough investigation.

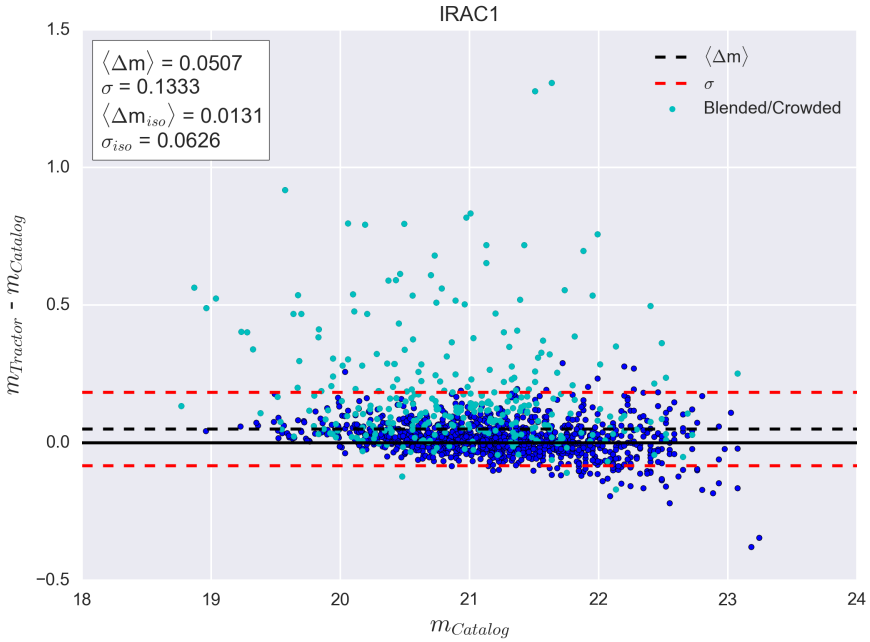

Figure 3: Comparison of extracted IRAC channel 1 photometry with the SERVS DR2 catalog values. Crowded sources are indicated as such. $\langle \Delta m \rangle$ and σ are given for both the whole comparison sample, as well as just for sources that are not crowded (i.e. isolated).

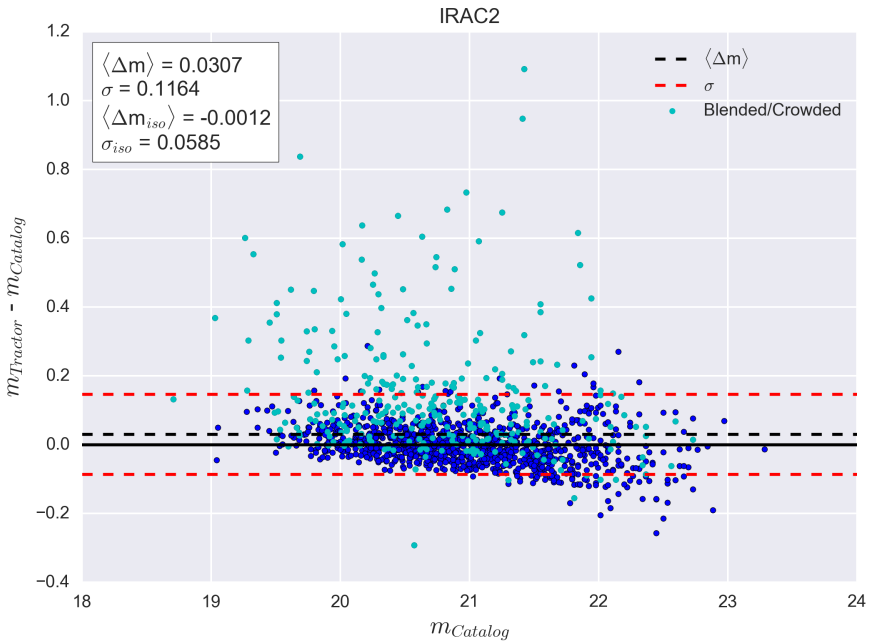

Figure 4: Comparison of extracted IRAC channel 2 photometry with the SERVS DR2 catalog values. Crowded sources are indicated as such. $\langle \Delta m \rangle$ and σ are given for both the whole comparison sample, as well as just for sources that are not crowded (i.e. isolated).

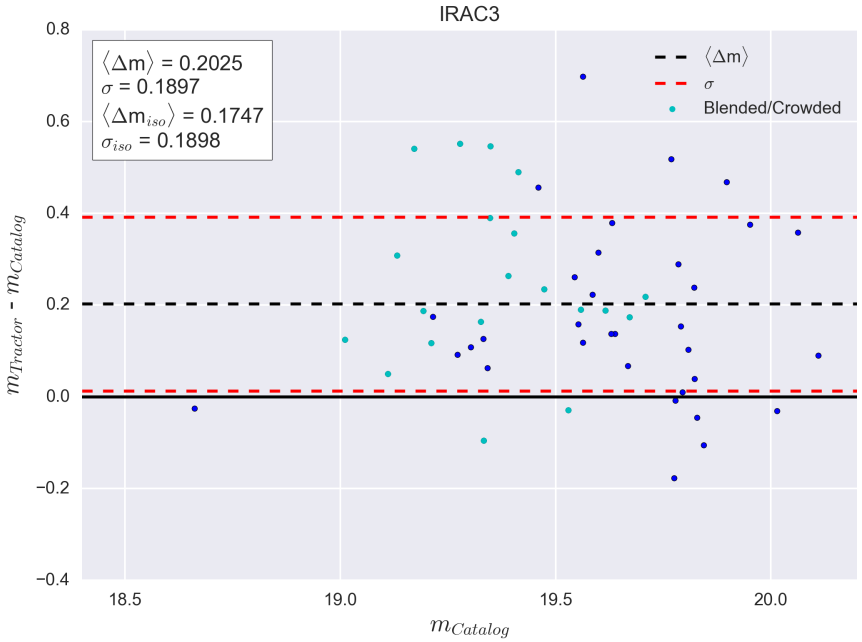

Figure 5: Comparison of extracted IRAC channel 3 photometry with the SWIRE DR2 catalog values. Crowded sources are indicated as such. $\langle \Delta m \rangle$ and σ are given for both the whole comparison sample, as well as just for sources that are not crowded (i.e. isolated).

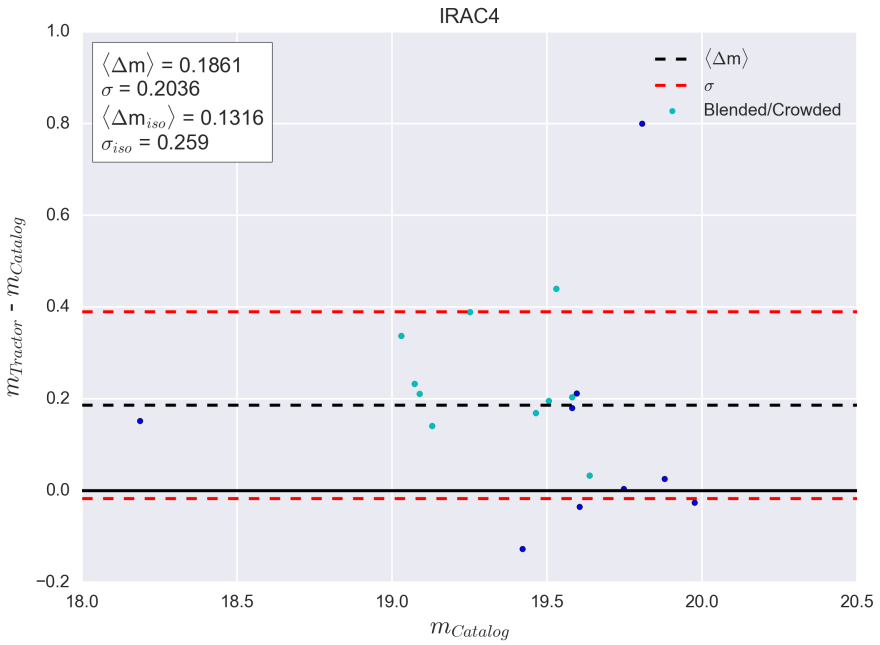

Figure 6: Comparison of extracted IRAC channel 4 photometry with the SWIRE DR2 catalog values. Crowded sources are indicated as such. $\langle \Delta m \rangle$ and σ are given for both the whole comparison sample, as well as just for sources that are not crowded (i.e. isolated).

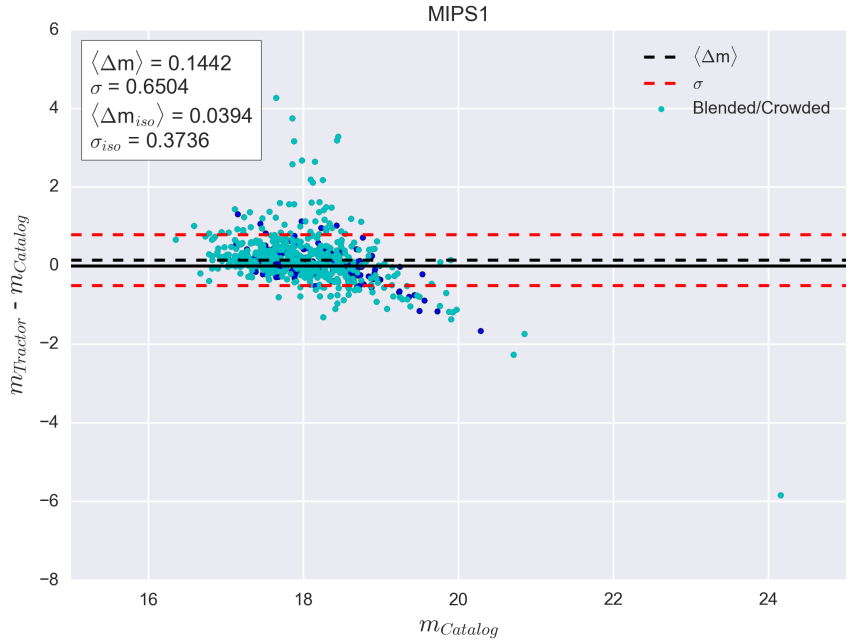

Figure 7: Comparison of extracted MIPS channel 1 photometry with the SWIRE DR2 catalog values. Crowded sources are indicated as such. $\langle \Delta m \rangle$ and σ are given for both the whole comparison sample, as well as just for sources that are not crowded (i.e. isolated).

When performing aperture photometry on a source that has a nearby neighbor, even if the source and the neighbor are not blended, the aperture placed around the primary source will contain a contribution from the bright outer rings of the neighbor's PSF. For this reason, crowded sources will be assigned a larger flux by aperture photometry than THE TRACTOR PSF-based photometry.

I define a source as being "crowded" if there is one or more other source(s) within two search radii ($\sim<$ FWHM) of the primary source. While blending (i.e. nearest neighbor lies within $\sim$ FWHM/2) does not become a critical issue until we consider the longest of wavelengths (here MIPS 24μm), source crowding occurs more frequently. Table 3 gives the fraction of the comparison sample that are crowded as well as the fraction of $\Delta m > \sigma$ outliers that are crowded.

Bandpass	Fraction Sample Crowded	Fraction ($\Delta m > \sigma$) Outliers Crowded
IRAC 1	22 %	91 %
IRAC 2	22 %	85 %
IRAC 3	38 %	50 %
IRAC 4	53 %	50 %
MIPS 1	70 %	88 %

Table 3: The fraction of the comparison sample that are crowded, and the fraction of the $\Delta m > \sigma$ outliers that are crowded

Clearly, the majority of outliers where the catalog flux is significantly greater than THE TRACTOR flux can be explained by source crowding. Further increasing the crowding radius criterion can explain an even larger fraction of the $\Delta m > \sigma$ outliers; however, too large of a radius will overestimate how much more distant neighbors influence the photometry of the primary source. I choose the conservative crowding radius of

$\sim>$ FWHM simply to demonstrate the effect of crowding and show that these outliers are not primarily due to THE TRACTOR performing poorly. Crowded and blended sources are indicated as such in Figures 3 through 7.

4.1.2 Flux Error

The table below summarizes the estimated errors in the extracted fluxes as calculated in Section 3.3. The catalog flux errors are the median aperture 2 flux errors in the catalogs associated with the corresponding image (SERVS for Ch. 1 and 2, SWIRE for Ch. 3, 4, and MIPS 24 μm).

Bandpass	N	$\sigma_{F,noise}$ [μJy]	$\widetilde{\sigma_{F,fit}}$ [μJy]	$\widetilde{\sigma_{F,tot}}$ [μJy]	Catalog $\widetilde{\sigma_F}$ [μJy]
IRAC 1	43.82	0.1394	0.1391	0.1969	0.4000
IRAC 2	42.58	0.1675	0.1671	0.2366	0.5000
IRAC 3	59.49	4.023	4.013	5.682	5.360
IRAC 4	72.11	4.798	4.846	6.819	5.940
MIPS 1	139.1	18.52	5.231	19.24	23.47

Table 4: The noise pixels, the noise contribution to the flux error, the median TRACTOR fit error, the median estimate of the total flux error, and the median catalog error for each bandpass.

The derived flux errors for IRAC channels 1 and 2 are a factor ~ 2 smaller than the median flux error in the SERVS catalog. The derived flux errors for IRAC channels 3, 4 and MIPS 24 μm are consistent with the SWIRE catalog flux errors.

4.2 Failure Indications

While a comparison of the extracted fluxes with the catalog values can indicate whether THE TRACTOR is failing to recover the source flux, it is not the only method of determining if and where THE TRACTOR has failed. My code also outputs the RMS of the total residual subimage, as well as the RMS of the individual fit of the central source (i.e. THE TRACTOR error). Large RMS values, relative to the median value for the sample, can indicate whether the subimage was poorly cleaned or the central source was poorly fit. The former is especially useful in determining whether a source in the subimage was "missed". Figures 8 through 12 give the distribution of the residual image RMS, distribution of THE TRACTOR error, and diagnostic plots demonstrating how offset, residual image RMS / THE TRACTOR error, and catalog magnitude are related.

I define bright (faint) sources as sources brighter (fainter) than the median magnitude of the comparison sample in each bandpass. It is apparent from Figures 8 through 12, that brighter sources are generally associated with a larger residual image RMS and TRACTOR error. This trend is less obvious in IRAC channels 3, 4 and MIPS channel 1 as the catalogs for these bandpasses are limited to brighter sources.

Extractions with large residual image RMS and TRACTOR error tend to be among those with large offsets. However, while a large residual image RMS or TRACTOR error does imply poorly fitted data, it does not necessarily indicate a large offset. Many of the sources with larger error indicators still reproduce the catalog flux. In this respect, a smaller residual image RMS or TRACTOR error does not guarantee that THE TRACTOR flux agrees with the catalog value. The diagnostic diagrams do not provide robust cuts that flag where THE TRACTOR has failed, but do provide some insight into where the code is succeeding or failing.

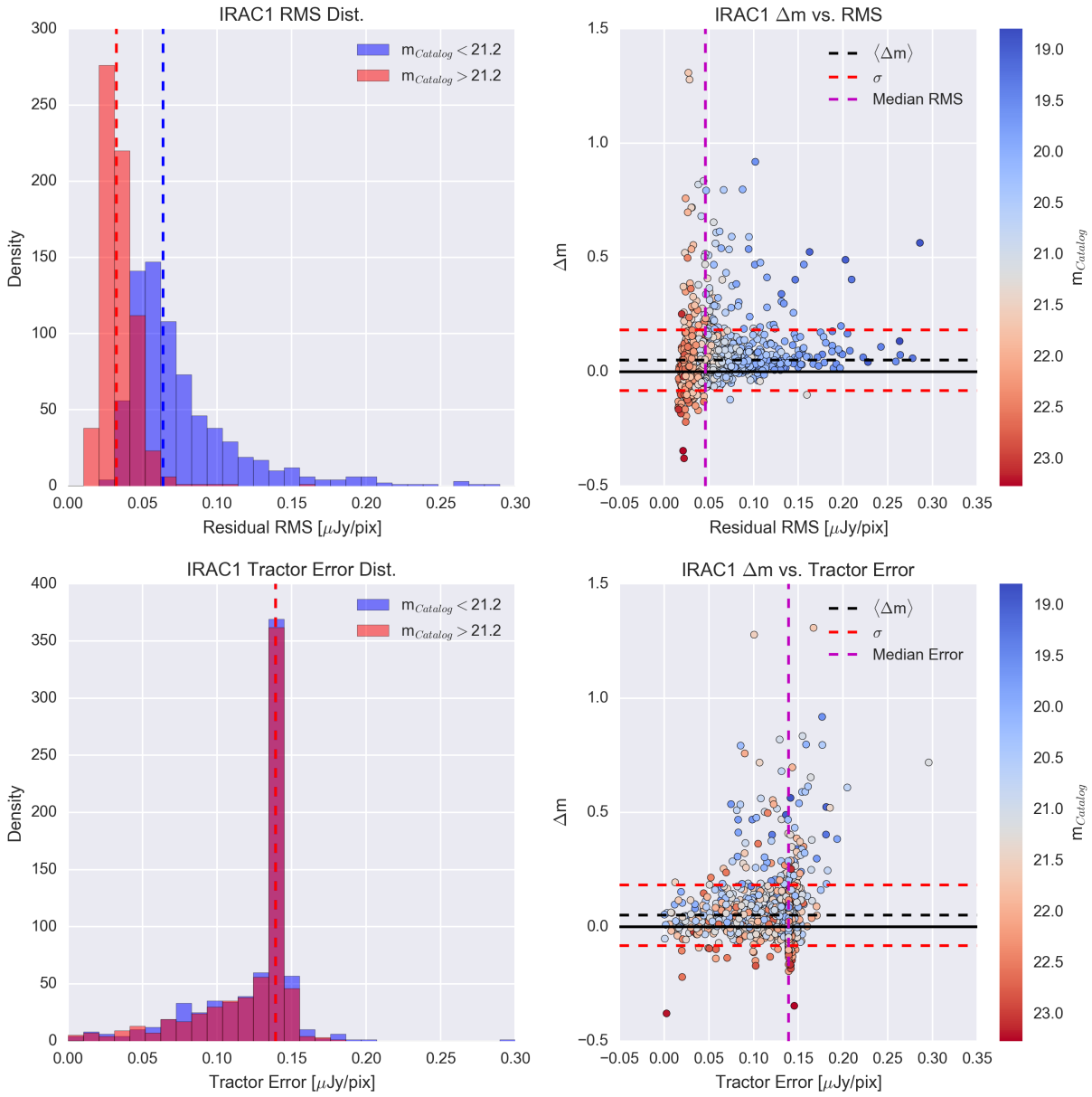

Figure 8: Top Left: Residual image RMS distribution for faint and bright sources with respect to the median magnitude of the sample. The median residual image RMS for each subset is indicated by a dashed vertical line. Top right: Diagnostic diagram illustrating how Δm, residual image RMS, and catalog magnitude are related. The median residual image RMS of the whole comparison sample is indicated by a dashed magenta line. The color bar is centered on the median magnitude of the comparison sample separating bright and faint sources. The bottom panels are the same plots, but with THE TRACTOR error in place of the residual image RMS.

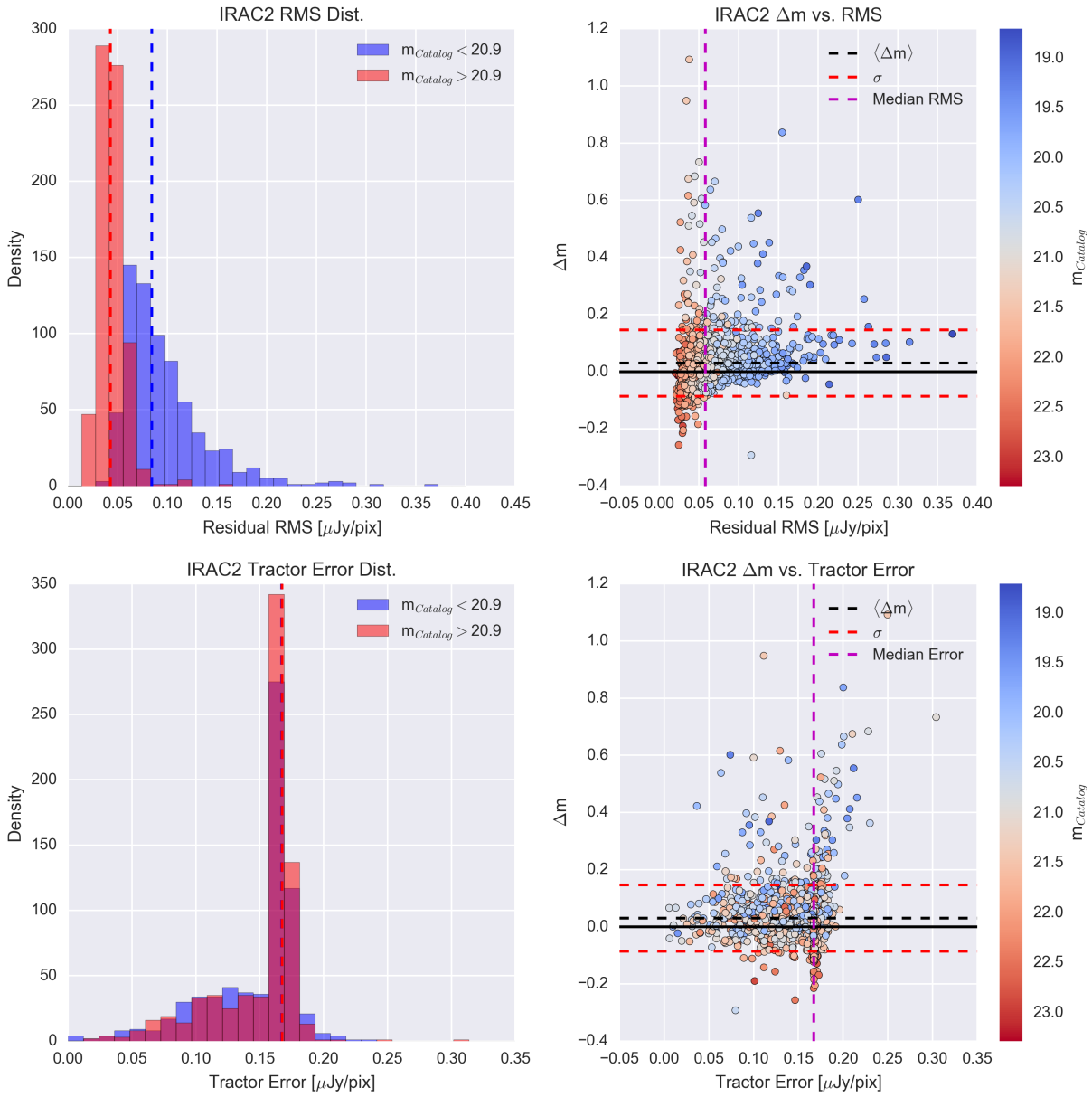

Figure 9: Top Left: Residual image RMS distribution for faint and bright sources with respect to the median magnitude of the sample. The median residual image RMS for each subset is indicated by a dashed vertical line. Top right: Diagnostic diagram illustrating how Δm, residual image RMS, and catalog magnitude are related. The median residual image RMS of the whole comparison sample is indicated by a dashed magenta line. The color bar is centered on the median magnitude of the comparison sample separating bright and faint sources. The bottom panels are the same plots, but with THE TRACTOR error in place of the residual image RMS.

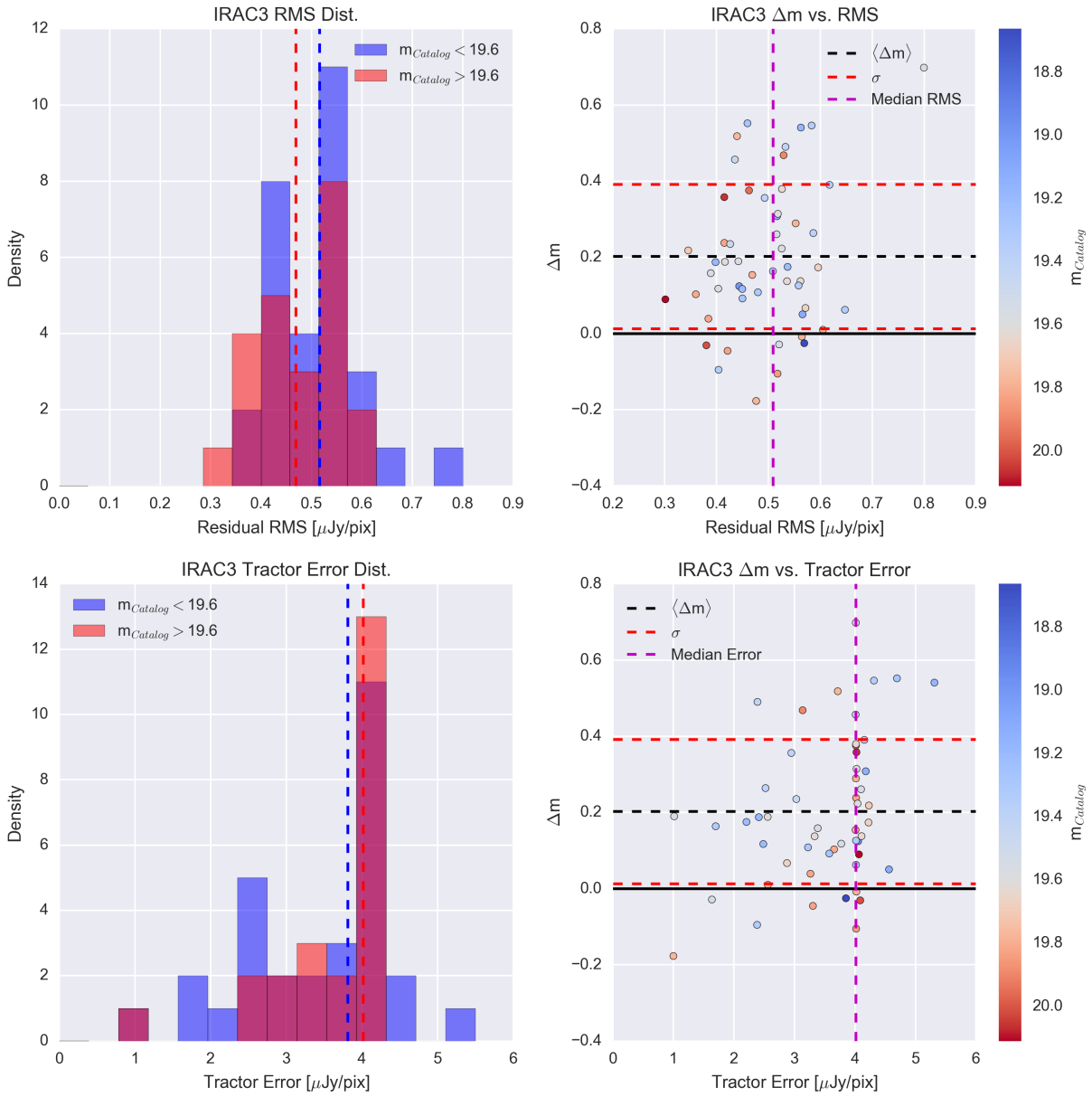

Figure 10: Top Left: Residual image RMS distribution for faint and bright sources with respect to the median magnitude of the sample. The median residual image RMS for each subset is indicated by a dashed vertical line. Top right: Diagnostic diagram illustrating how Δm, residual image RMS, and catalog magnitude are related. The median residual image RMS of the whole comparison sample is indicated by a dashed magenta line. The color bar is centered on the median magnitude of the comparison sample separating bright and faint sources. The bottom panels are the same plots, but with THE TRACTOR error in place of the residual image RMS.

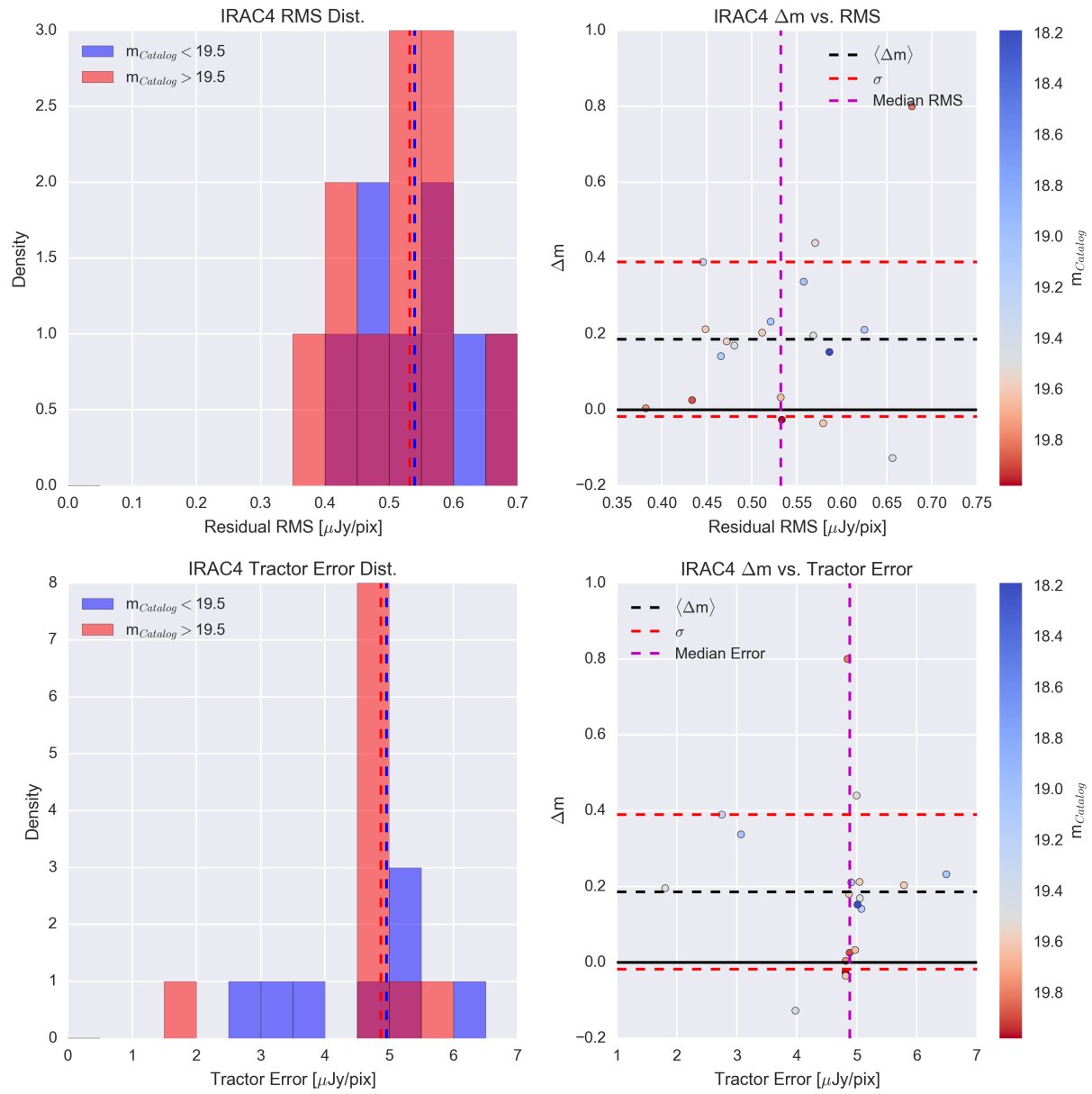

Figure 11: Top Left: Residual image RMS distribution for faint and bright sources with respect to the median magnitude of the sample. The median residual image RMS for each subset is indicated by a dashed vertical line. Top right: Diagnostic diagram illustrating how Δm, residual image RMS, and catalog magnitude are related. The median residual image RMS of the whole comparison sample is indicated by a dashed magenta line. The color bar is centered on the median magnitude of the comparison sample separating bright and faint sources. The bottom panels are the same plots, but with THE TRACTOR error in place of the residual image RMS.

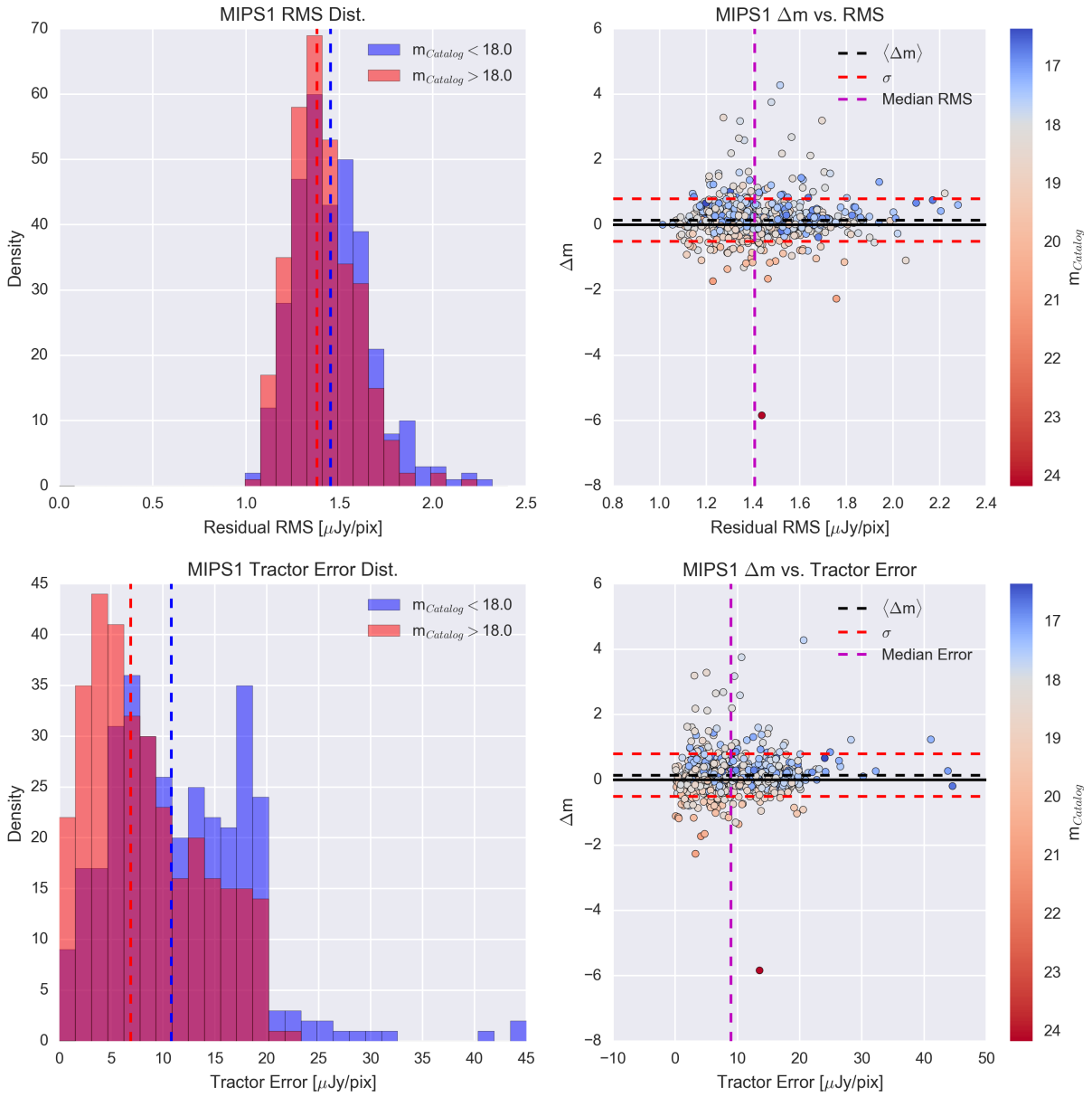

Figure 12: Top Left: Residual image RMS distribution for faint and bright sources with respect to the median magnitude of the sample. The median residual image RMS for each subset is indicated by a dashed vertical line. Top right: Diagnostic diagram illustrating how Δm, residual image RMS, and catalog magnitude are related. The median residual image RMS of the whole comparison sample is indicated by a dashed magenta line. The color bar is centered on the median magnitude of the comparison sample separating bright and faint sources. The bottom panels are the same plots, but with THE TRACTOR error in place of the residual image RMS.

4.3 Failed Methods

In principle, one can allow all image and source parameters to vary to optimize the fit. In practice, allowing too many parameters to vary often lead to unphysical fits with respect to one or more of the parameters or caused THE TRACTOR to crash. Fixing one or more of the parameters during the fitting procedure improved results for some cases, but also lead to other problems. For example, fixing the axis ratio and position angle parameters of the source shape lead to large, unphysical radii for more elongated sources and sources in noisy regions. Similarly, letting position vary occasionally lead to large changes in position. The current version of THE TRACTOR (1.0) does not allow the user to constrict the ranges for fit parameters.

Strategies where only flux was allowed to vary (*forced photometry*) led to some success, albeit sometimes for the wrong reasons. One method attempted was to approximate the PSF model to a circular Gaussian and the source model to a fixed circular disk. I was able to modify the projected radius of that disk until my fluxes agreed with the catalog values. These shapes were not physically motivated, but rather were used to expand or compress the Gaussian PSF such that it would extract the catalog flux values I was aiming for. I found that while I would change the FWHM of the Gaussian PSF model from bandpass to bandpass according to the *Spitzer* Instrument Manual, one fixed projected shape did not succeed uniformly at all wavelengths. Furthermore, at longer wavelengths, a pure Gaussian PSF model is no longer a good approximation to the true PSF as the bright outer rings of the true PSF become non-negligible.

The most recent method preceding the one outlined in Section 3, involved assuming the source to be a point source, modeling the PSF as a circular Gaussian, and deriving a pseudo-aperture correction for the flux that was being missed by the PSF model. Again, assuming the source to be a point source allowed me to bypass having to model the projected shape and surface brightness profile of each source. The results for this method varied. This method assumed that THE TRACTOR would, in an identical manner, fit the same central portion of the image PSF for all sources, which I'm not sure is the case. The aperture correction was difficult to accurately estimate due to the aforementioned potential variability of the fit of the central portion of the PSF, as well as the variability in the sky background.

5 Summary

The method described in this article has been the most successful of all of the methods I have attempted, and requires the least number assumptions regarding the image and source priors i.e. the key assumption is that the sources are unresolved. I adopted K_S position priors, IRAC and MIPS flux priors, and PSF models derived in the literature for the corresponding instruments to ensure my best estimate of the source fluxes.

The best agreement between my extracted fluxes and the catalog values occurs in IRAC channel 2 with $\langle \Delta \mathrm{m}_{iso} \rangle$ = -0.0012 and σ_{iso} = 0.0585, while the worst agreement occurs in IRAC channel 3 with $\langle \Delta \mathrm{m}_{iso} \rangle$ = 0.1747 and σ_{iso} = 0.1898; though, the samples compared in IRAC channels 3 and 4 are likely too small (53 and 19 sources) to be indicative of the results of a larger scale comparison.

Adopting the true PSF has been the primary improvement to my photometry method. This will also likely improve results in cases where the sources are resolved and the projected shape and profile of the source must be modeled.

6 Examples

Below are some examples of successful and failed fits by THE TRACTOR in each bandpass as indicated by the residual image RMS. The red crosses indicate the prior position, and the green x's indicate the final fit position. Because the position was held fixed during the fitting procedure, these are at the same position. Note: the units on the color bars are in the map units [MJy/sr].

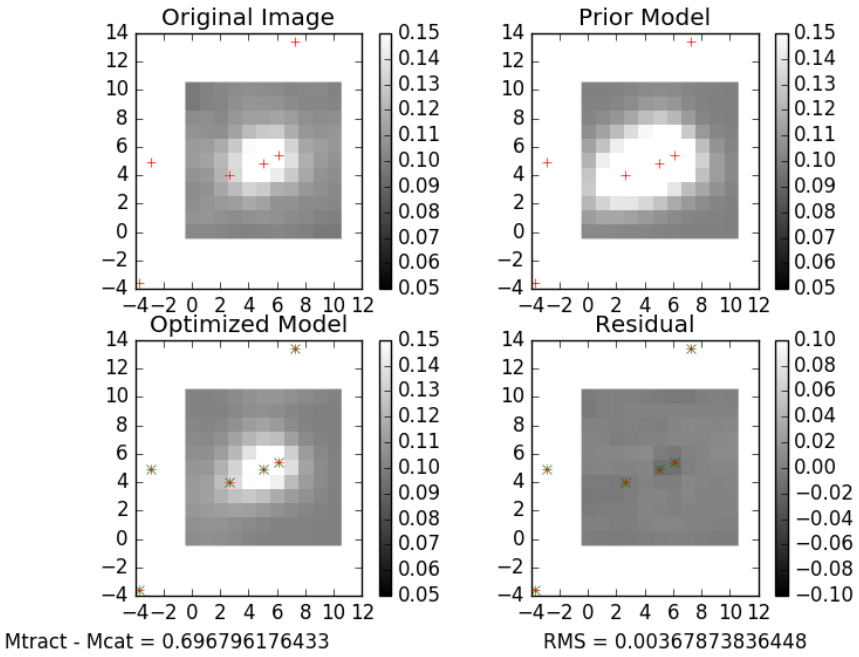

Figure 13: HIERO21: THE TRACTOR deblends this single IRAC channel 1 source into 3 fainter sources. As a result the extracted flux of the central source is less than the value in the catalog.

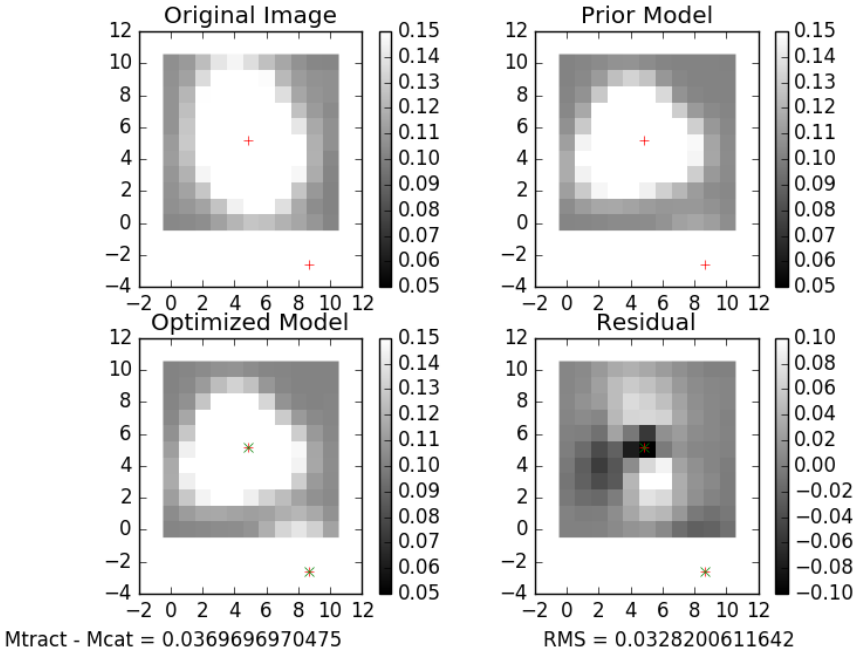

Figure 14: HIERO126: this IRAC channel 1 source is elongated and so the pure PSF fitting method does not fit the source well. Though, the catalog flux is still approximately recovered.

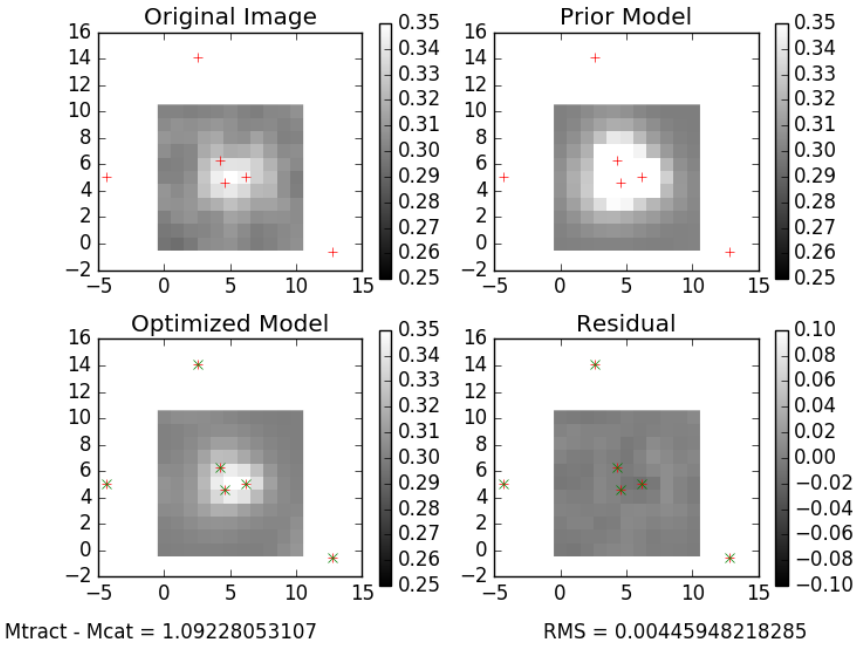

Figure 15: HIERO225: THE TRACTOR deblends this single IRAC channel 2 source into 3 fainter sources. As a result the extracted flux of the central source is less than the value in the catalog.

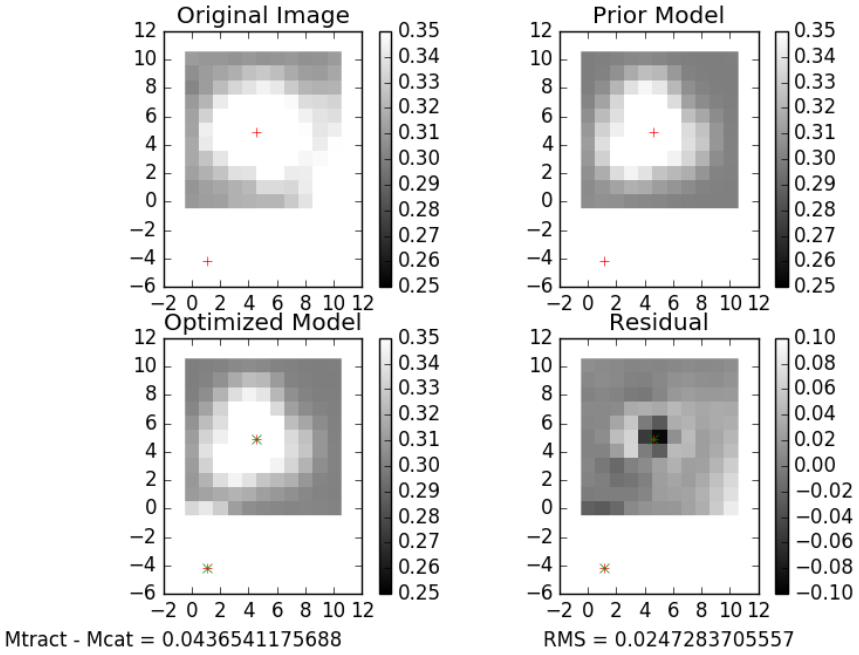

Figure 16: HIERO1257: THE TRACTOR over-extracts this IRAC channel 2 source as indicated by the negative pixel values in the center of the source in the residual image. The code is trying to compensate for the additional light contributed by the "missed" bright source in the lower right corner.

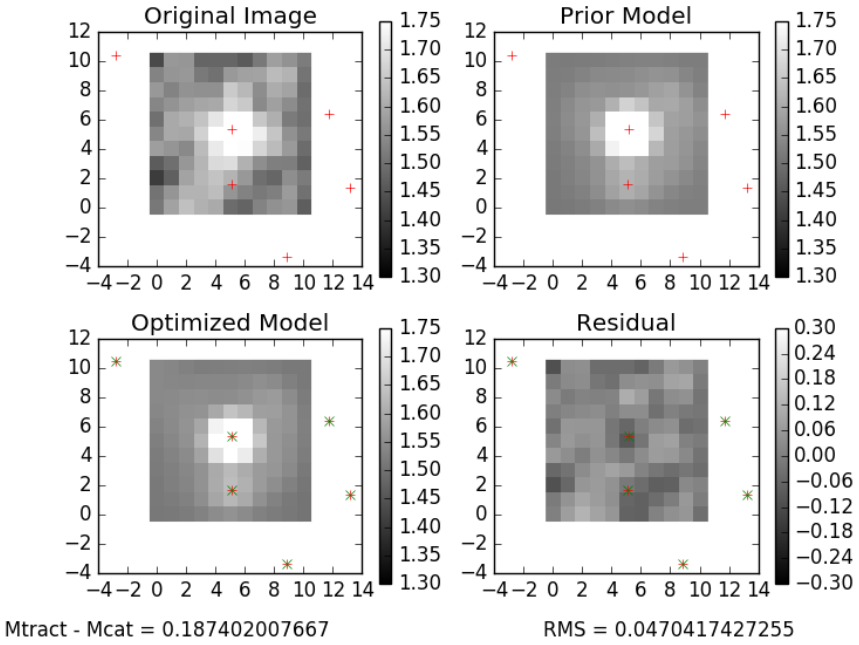

Figure 17: HIERO1066: this IRAC channel 3 source has a nearby neighbor and so we would expect the extracted flux of this source to be less than the catalog value (see Section 4.1.1). The Tractor correctly accounts for the flux contribution from the nearby neighbor.

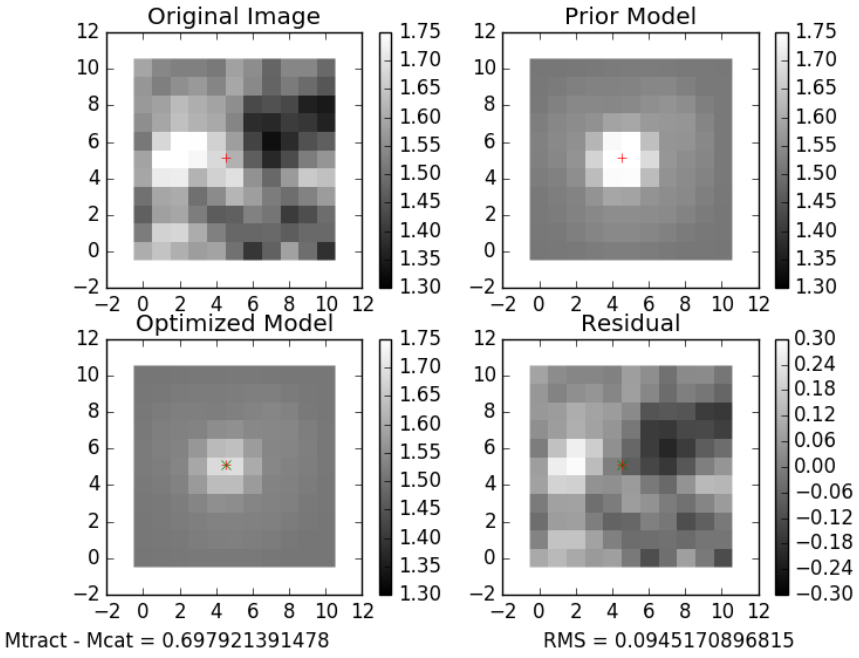

Figure 18: HIERO1297: For this IRAC Channel 3 source, it appears that either there is some positional error between the K_S catalog and the SWIRE image, or an IRAC channel 3 source was not present in the K_S catalog to obtain a position prior.

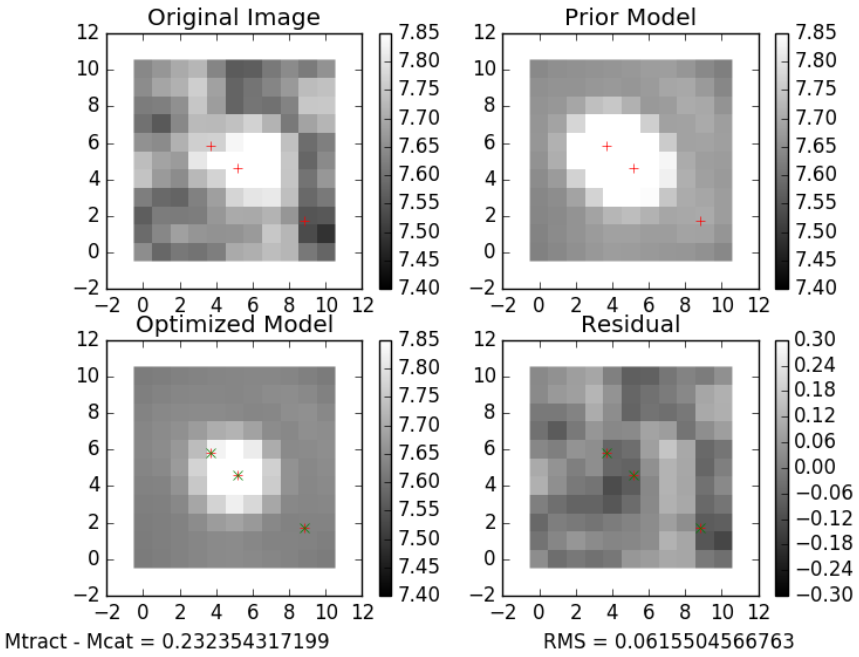

Figure 19: HIERO1116: this IRAC channel 4 source is deblended into 2 fainter sources by THE TRACTOR. As a result, the extracted flux is less than the value in the catalog.

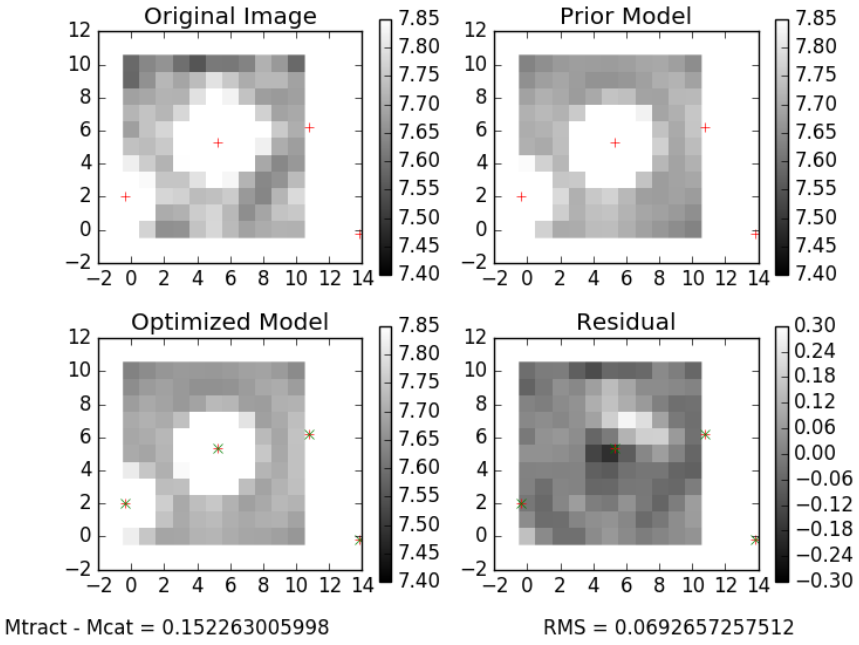

Figure 20: KIERO406: THE TRACTOR leaves behind some residual flux for this IRAC channel 4 source.

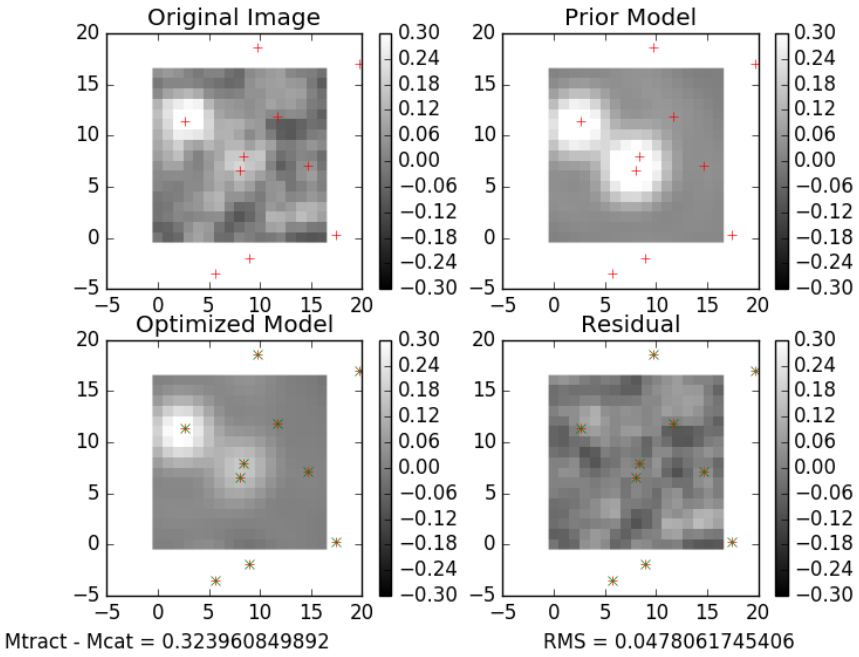

Figure 21: HIERO658: THE TRACTOR performs well on this MIPS 24 μm source that is not only blended, but has an additional nearby neighbor. As expected, THE TRACTOR flux is less than the value in the catalog.

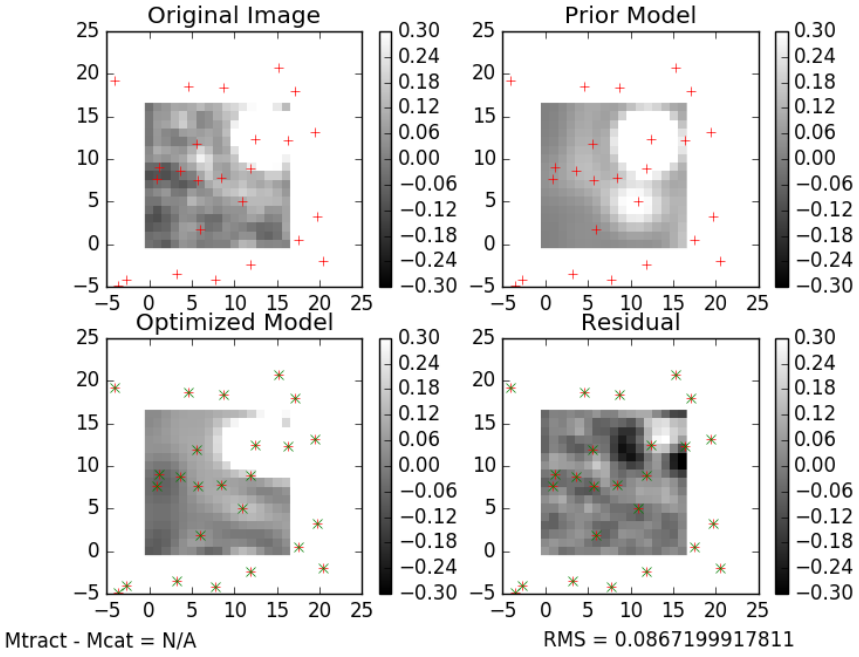

Figure 22: HIERO980: THE TRACTOR assigns the central source a negative MIPS 24 μm flux due to THE TRACTOR's failure to robustly extract the nearby bright source in the image.

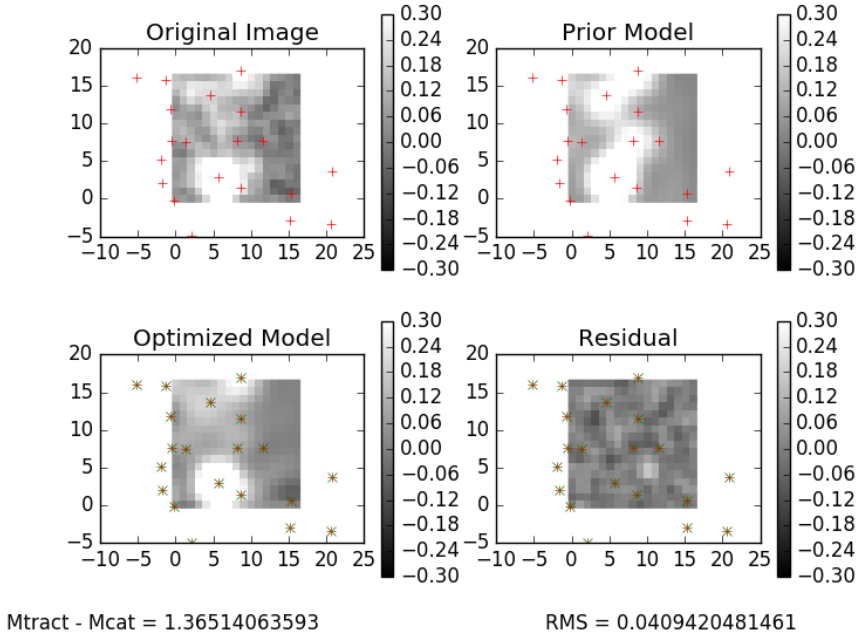

Figure 23: HIERO190: this additional MIPS 24 μm example demonstrates the ability of THE TRACTOR to clean even the most crowded images.